RSC Advances

PAPER

View Article Online
View Journal | View Issue

Cite this: *RSC Adv.*, 2020, **10**, 8261

Colloidal quantum dot light-emitting diodes employing solution-processable tin dioxide nanoparticles in an electron transport layer

Myeongjin Park,[a] Jiyun Song,[a] Myungchan An,[b] Jaehoon Lim,[c] Changhee Lee,[a] Jeongkyun Roh *[d] and Donggu Lee*[b]

Received 21st January 2020
Accepted 19th February 2020

DOI: 10.1039/d0ra00653j

rsc.li/rsc-advances

Colloidal quantum-dot-based light-emitting diodes (QD-LEDs) have gained tremendous attention as great candidates to potentially replace current emissive display technologies. The luminescence efficiency of a QD LED has increased rapidly in the past decade; this was triggered by the use of metal oxides in the charge transport layers, particularly zinc oxide (ZnO) for the electron transport layer (ETL). However, the ZnO ETL often results in undesirable device performance such as efficiency roll-off and poor device stability because of excessive electron injection into the QD emissive layer. Here, we explore solution-processable tin dioxide (SnO_2) nanoparticles (NPs) as alternatives to ZnO NPs for the ETL in QD-LEDs. We evaluated the thin-film quality and electrical performance of SnO_2 NPs and then applied them to the ETL for constructing QD-LEDs. As a result of the smooth surface morphology, moderate electron-transport ability, and lower carrier concentration compared to ZnO NPs, the QD-LED with SnO_2 NP-ETL exhibited improved performance in terms of lower turn-on and operating voltages, maximum luminance, improved efficiency roll-off, and improved power efficiency over the reference device with the ZnO NP-ETL. This shows promising potential for SnO_2 NPs in optoelectronic applications.

Introduction

Colloidal quantum dots (QDs) are considered a key material for next-generation displays because of their excellent optical properties such as tunable emission wavelength, high color purity, and high photoluminescence (PL) quantum yield.[1–3] These unique features have enabled successful commercialization of QD display technologies based on color enhancement films. Intense research works are presently underway as the next step toward replacement of current emissive displays by QD light-emitting diodes (QD-LEDs). Luminescence efficiency is one of the most important factors in the commercialization of QD-LEDs. Through careful studies on the design of QDs, the PL quantum yield has almost reached 100%, indicating high technological advancement in QD synthesis.[4,5] Simultaneously, several studies have been conducted to achieve high luminescence efficiency from an electroluminescence (EL) device *via* optimum device architecture. This involves finding suitable materials for the charge transport layers (CTLs) and charge injection layers (CILs) of electrons and holes, and various types of organic/inorganic nanomaterials have been employed and investigated.[6–8] Among these materials, zinc oxide (ZnO) nanoparticles (NPs) have been most frequently employed as electron transport layers (ETLs) because of their excellent electron mobilities and suitable energy levels for efficient electron injection.[9–11] Although ZnO ETLs are widely employed and considered a standard platform for high-efficiency QD-LEDs, ZnO has been often indicated as the main reason for undesirable behavior of QD-LED performance such as efficiency roll-off, EL quenching, and short lifetime.[12–14] These behaviors are attributable to excessive electron injection from ZnO into the QDs, which lead to non-balancing of electron and hole densities in the QD emissive layer.[15] To move one step closer to commercialization, it is currently necessary to study other alternatives that can potentially supplement or even replace ZnO.

In this study, we explore tin dioxide (SnO_2) NPs as possible alternatives to ZnO NPs for ETLs in QD-LEDs. SnO_2 NPs are solution-processable n-type semiconductors similar to ZnO NPs and can form transparent and smooth thin films at temperatures below 100 °C. SnO_2 NPs. In addition, they possess a wider bandgap with less sensitivity in the ultraviolet regime than ZnO, indicating better light stability.[16] Because of their superior features, SnO_2 have been often employed in perovskite photovoltaics as an alternative of TiO_2,[17–19] but utilization of SnO_2 in

[a]*Department of Electrical and Computer Engineering, Inter-university Semiconductor Research Center, Seoul National University, Seoul 08826, Republic of Korea*

[b]*Realistic Media Research Center, Innovative Technology Research Division, Gumi Electronics & Information Technology Research Institute (GERI), Gumi 39253, Republic of Korea. E-mail: dglee@geri.re.kr*

[c]*Department of Energy Science, Center for Artificial Atoms, Sungkyunkwan University (SKKU), Suwon-Si, Gyeonggi-do 16419, Republic of Korea*

[d]*Department of Electrical Engineering, Pusan National University, Busan, 46241, Republic of Korea. E-mail: jkroh@pusan.ac.kr*

LEDs has not been performed. To test the suitability of SnO_2 NPs for ETLs, we first evaluated the thin-film quality of SnO_2 NPs using atomic force microscopy (AFM) measurements, and confirmed that SnO_2 NPs form uniform thin films without notable valleys. Then, we investigated the electrical properties of SnO_2 NPs, such as electron mobility and carrier concentration, by employing a field-effect transistor (FET) as a test platform. Finally, we constructed QD-LEDs based on an inverted structure using SnO_2 NPs for the ETL, evaluated the device performance, and compared it to that of QD-LEDs with the ZnO NP-ETL.

Experimental

Materials

The SnO_2 NPs dispersed in water (>99.5%) was purchased from MKnano and used as received. The synthetic procedure for ZnO nanoparticles and CdSe/CdS/CdZnS red QDs followed a reported method by Kawk *et al.*[9] Precursors for synthesizing QDs and ZnO nanoparticles (zinc acetate dehydrate > 99%, tributylphosphine > 99%, 1-octadecene > 95%, trioctylphosphine > 97%, oleic acid > 99%) were purchased from Sigma-Aldrich, and potassium hydroxide (>85%) was purchased from Duksan Pharmaceutical Co. Ltd.

Characterization of ZnO and SnO_2 films

An Agilent 8454 UV-visible spectrometer was used for UV-vis absorption. An XE-100 (Park Systems Corp.) AFM system was used to analyze the topography of the ZnO NPs and SnO_2 NP films. The transmission electron microscopy (TEM) images of the ZnO and SnO_2 NPs were taken with a JEOL JSM-890 at an accelerating voltage of 120 kV.

Fabrication and characterization of FETs based on metal oxide NPs

Heavily doped silicon and thermally grown 300 nm SiO_2 were used as a gate and gate dielectric, respectively. The Si/SiO_2 substrates were cleaned in an ultra-sonication bath with acetone, isopropyl alcohol, and de-ionized water, sequentially. Then, the substrates were stored in a vacuum oven for 10 min to remove moisture. Before depositing metal-oxide NPs, the substrates were UVO-treated for 10 min, and then ZnO or SnO_2 NPs were spin-coated onto the substrates. Then, the metal oxide NP films were annealed at 90 °C for 30 min to remove residual solvents. A shadow mask was used to form source and drain electrodes by thermally evaporating 0.5 nm LiF and 100 nm Al, sequentially. The channel width and length of the FETs were 65 μm and 1800 μm, respectively. The electrical performance of metal-oxide NP-based FETs were measured using a semiconductor parameter analyzer, Agilent 4155C.

Fabrication and characterization of QD-LEDs

Patterned ITO glass substrates were sequentially ultrasonicated with acetone, isopropanol, and deionized water for at least 5 minutes. Then, the cleaned substrates were dried in an oven at 120 °C for at least 30 min. To deposit the electron injection layer, a SnO_2 NP solution (15 mg mL^{-1} dispersed in deionized water) and a ZnO NP solution (20 mg mL^{-1} in butanol) were spin-casted on the substrate, respectively, at 2000 rpm for 60 s. The coated films were baked in a N_2 oven at 90 °C for 30 min, and the thickness measured with an ellipsometer was 40 nm. After baking, a 20 mg mL^{-1} QD solution in hexane was spin-casted on top of the ETL at 4000 rpm for 30 s, and then baked again in the N_2 oven at 70 °C for 30 min to form a 20 nm emissive layer. Finally, the substrates were transferred to a vacuum evaporator, and then 40 nm CBP for the hole transport layer (HTL), 10 nm MoO_3 for the hole injection layer (HIL) and 100 nm Al for the anode were thermally evaporated with a deposition rate of 1 A s^{-1}. The current density–voltage–luminance (*J–V–L*) characteristics were measured using a Keithley 236 source-measurement unit and calibrated Si photodiode (Hamamatsu, S5227-1010BQ). During the *J–V* measurement, luminance was obtained by correcting the photocurrent of the Si photodiode with a luminance value measured by a spectroradiometer (Konica-Minolta CS-1000A).

Results and discussion

Fig. 1 shows a schematic illustration of inverted-structure QD-LEDs with ETLs consisting of metal-oxide NPs. The metal-oxide NPs used in this study, ZnO and SnO_2, had a similar size of ~3–5 nm as shown in the TEM images in Fig. 1. In this inverted structure, metal-oxide NPs were deposited on the bottom ITO electrode, and QDs were deposited on top of the metal-oxide NP ETLs. Thus, it is extremely important to have high-quality metal-oxide NP films because (i) the morphology of the QD emissive layer follows the morphology of the underlying ETL; and (ii) pinholes or cracks present in the ETL result in the direct contact of QDs with the bottom electrode which yields a massive leakage current. To evaluate the thin-film quality of SnO_2 NPs, we performed AFM measurements for both SnO_2 and ZnO NP films and compared them accordingly.

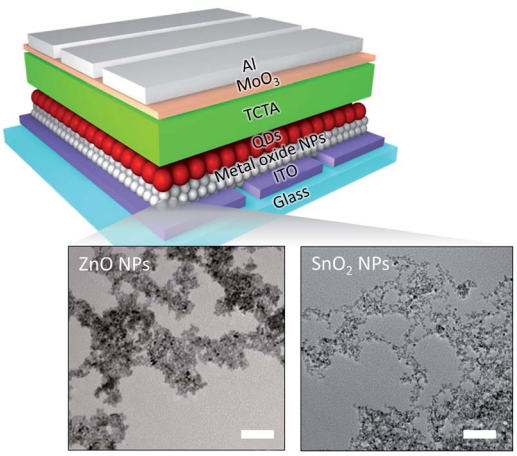

Fig. 1 Schematic illustration of the QD-LED based on an inverted structure with an ETL consisting of metal-oxide NPs. Bottom inset shows TEM images of metal-oxide NPs used in this study. The scale bars represent 50 nm.

Fig. 2(a) and (b) show the surface morphology of the thin films consisting of ZnO and SnO_2 NPs, respectively. As shown, SnO_2 NPs produce a smooth, thin film without notable cracks or a valleys, similar to ZnO NPs. The surface roughness of the SnO_2 NP film measured by rms over the 5 μm × 5 μm area is 2.8 nm, which is lower than that of the ZnO NP film (3.9 nm). The high smoothness of the SnO_2 NP film is a favorable feature for ETLs, which is linked to a lower leakage current, high EL efficiency (*i.e.*, a uniform emissive layer), maximum luminescence (*i.e.*, high breakdown voltage), and high device stability.

After confirming the high film quality of the SnO_2 NPs, we evaluated its electrical properties using an FET platform. An FET is a representative electronic device that can amplify or switch signals; it is also a useful platform with which to evaluate the electrical properties of semiconductors. As shown in Fig. 3(a), we fabricated bottom-gate top-contact FETs using ZnO or SnO_2 NPs as the channel material. Fig. 3(b) shows the transfer characteristics of the FETs based on ZnO and SnO_2 NPs in a saturation regime with a drain-to-source voltage (V_{DS}) of 100 V. The electron mobility and threshold voltage can be extracted from the equation,

$$I_{DS} = \frac{1}{2}\mu_{FET} C_{GI} \frac{W}{L}(V_{GS} - V_{TH})^2 \quad (1)$$

where μ_{FET} is the field-effect mobility; C_{GI} the capacitance of the gate insulator; W and L the channel width and length, respectively; and V_{GS} the gate-to-source voltage. By taking the square roots of both sides and plotting, we can extract mobilities and threshold voltages from the slope and x-intercept of the graphs, respectively. The extracted mobilities of the ZnO and SnO_2 NPs are 2.91 × 10^{-4} cm^2 V^{-1} s^{-1} and 2.83 × 10^{-4} cm^2 V^{-1} s^{-1}, respectively. The similar electron mobility of SnO_2 NPs to ZnO NPs indicate the similar electron-transporting ability of SnO_2 NPs. In contrast to the electron mobility, however, the SnO_2 NP-based FETs showed a considerably higher threshold voltage of 34.3 V than that of the ZnO NP-based FETs, 2.16 V. The higher threshold voltage implies a higher required voltage to generate a conductive channel, which represents the lower carrier concentration of SnO_2 NPs than ZnO NPs. This can be reaffirmed by a quantitative analysis of the carrier concentration of metal-oxide NPs. The carrier concentration (N_e) can be calculated from the conductivity (σ) of each channel according to the relationship $N_e = \sigma/q\mu_{FET}$, where q is the elementary charge. The conductivity of each material was obtained using the previously suggested method,[20] and the obtained carrier concentrations were 6.89 × 10^{17} cm^{-3} and 3.11 × 10^{17} cm^{-3} for ZnO and SnO_2 NPs, respectively. The carrier concentration of SnO_2 NPs is half that of the carrier concentration of ZnO NPs, which corresponds to the higher threshold voltage in the FETs. The high carrier concentration of ZnO has often plagued the QD-LED performance and stability by quenching excitons and/or unbalancing carrier densities owing to excessive electron injection. In this regard, a lower carrier concentration of SnO_2 NPs may be more beneficial for the ETL in QD-LEDs. Note that SnO_2 NPs exhibit decent electron transporting ability as evidenced from the compatible electron mobility to ZnO NPs.

Finally, we fabricated QD-LEDs based on the SnO_2 NP-ETL as shown in Fig. 1. In this study, we employed CdSe/CdS/CdZnS red QDs with a high PL quantum yield of approximately 80%. Fig. 4(a) shows an energy diagram of the QD-LEDs with ETLs consisting of ZnO or SnO_2 NPs. As displayed in the figure, electrons injected from ITO pass through metal oxide NPs and arrive at the QD emissive layer, indicating that metal-oxide NPs play a significant role in both electron injection and transport. Fig. 4(b) shows the EL spectra of QD-LEDs with ZnO or SnO_2 NP-ETLs. The luminance–voltage–current density (L–V–J) measurements show that the QD-LED with the SnO_2 NP-ETL exhibits comparable or even slightly improved performance over the ZnO NP ETL-based device. Besides, the device with the SnO_2 NP-ETL shows a low driving voltage in the J–V curve compared to the ZnO NP-ETL device, denoting its suitability as an electron injection/transport layer. As a result, the device with the SnO_2 NP-ETL has a lower turn-on voltage (V_{ON} ∼ 2.15 V) and higher maximum luminance (L_{max} ∼ 15 000 cd m^{-2}) than the ZnO NP-ETL based device (V_{ON} ∼ 2.35 V, L_{max} ∼ 10 000 cd m^{-2}). Furthermore, as shown in Fig. 4(d), the QD-LED with the SnO_2

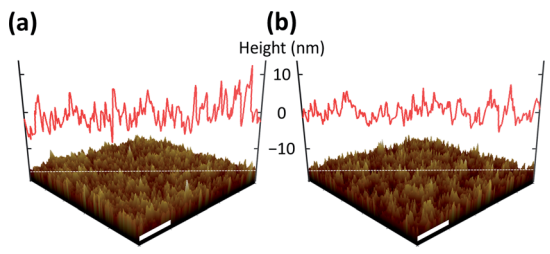

Fig. 2 AFM surface morphologies of thin films consisting of (a) ZnO NPs and (b) SnO_2 NPs along with their surface profiles. The scale bars represent 1 μm.

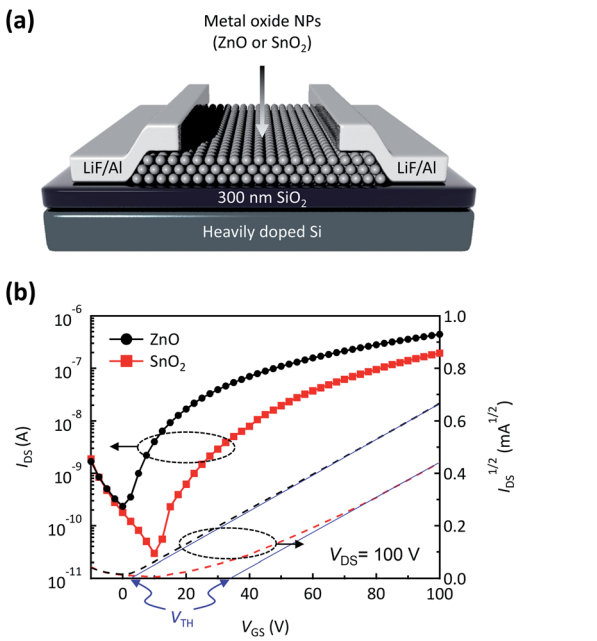

Fig. 3 (a) Device structure of FETs based on metal-oxide NPs. (b) Saturation-regime transfer characteristics of FETs based on ZnO and SnO_2 NPs. The blue arrows indicate x-intercepts which represent threshold voltages of each device.

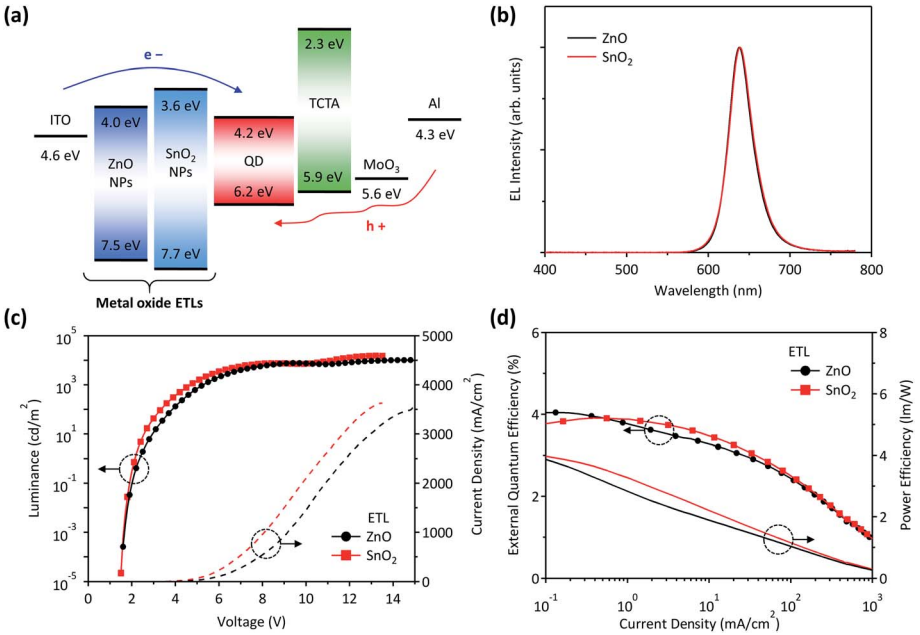

Fig. 4 (a) Energy diagram of QD-LEDs with metal-oxide NP-based ETLs. (b) EL spectra, (c) *L*–*V*–*J* characteristics, and (d) EQE and PE characteristics of devices with ZnO NP- and SnO_2 NP-ETLs.

NP-ETL exhibits improved external quantum efficiency (EQE) roll-off behavior with a peak EQE of 3.9% and power efficiency (PE) compared to the ZnO NP-ETL based device. This shows the excellent performance of the SnO_2 NPs for the ETL in QD-LEDs; this is attributable to the high thin-film quality, comparable electron mobility, and lower carrier concertation, which could suppress spontaneous electron injection.

Conclusions

In summary, we examined SnO_2 NPs for the ETL in QD-LEDs as a possible alternative to ZnO NPs. The high thin-film quality of the SnO_2 NPs is a favorable feature for ETL in preventing leakage current pathways, and its electrical performance, including the moderate electron mobility and lower carrier concentration than ZnO NPs, is desirable for the ETL in QD-LEDs. As a result, the QD-LEDs based on the SnO_2 NP-ETL show compatible or even improved device performance over the device to those with the ZnO NP-ETL; this indicates the promising potential of SnO_2 NPs as a supplement or an alternative to ZnO NPs. This work is expected to expand the utilization of SnO_2 NPs in optoelectronic applications and promote exploration of other types of metal-oxide NPs.

Conflicts of interest

There are no conflicts to declare.

Acknowledgements

This work was supported by the Ministry of Education of the Republic of Korea and the National Research Foundation of Korea (NRF-2019R1C1C1005258).

Notes and references

1 Y.-H. Won, O. Cho, T. Kim, D.-Y. Chung, T. Kim, H. Chung, H. Jang, J. Lee, D. Kim and E. Jang, *Nature*, 2019, **575**, 634–638.
2 H. Shen, Q. Gao, Y. Zhang, Y. Lin, Q. Lin, Z. Li, L. Chen, Z. Zeng, X. Li, Y. Jia, S. Wang, Z. Du, L. S. Li and Z. Zhang, *Nat. Photonics*, 2019, **13**, 192–197.
3 P. O. Anikeeva, J. E. Halpert, M. G. Bawendi and V. Bulović, *Nano Lett.*, 2009, **9**, 2532–2536.
4 D. A. Hanifi, N. D. Bronstein, B. A. Koscher, Z. Nett, J. K. Swabeck, K. Takano, A. M. Schwartzberg, L. Maserati, K. Vandewal, Y. van de Burgt, A. Salleo and A. P. Alivisatos, *Science*, 2019, **363**, 1199.
5 B. G. Jeong, Y.-S. Park, J. H. Chang, I. Cho, J. K. Kim, H. Kim, K. Char, J. Cho, V. I. Klimov, P. Park, D. C. Lee and W. K. Bae, *ACS Nano*, 2016, **10**, 9297–9305.
6 J. M. Caruge, J. E. Halpert, V. Wood, V. Bulović and M. G. Bawendi, *Nat. Photonics*, 2008, **2**, 247–250.
7 M. D. Ho, D. Kim, N. Kim, S. M. Cho and H. Chae, *ACS Appl. Mater. Interfaces*, 2013, **5**, 12369–12374.
8 V. Wood, M. J. Panzer, J. E. Halpert, J. M. Caruge, M. G. Bawendi and V. Bulović, *ACS Nano*, 2009, **3**, 3581–3586.
9 J. Kwak, W. K. Bae, D. Lee, I. Park, J. Lim, M. Park, H. Cho, H. Woo, D. Y. Yoon, K. Char, S. Lee and C. Lee, *Nano Lett.*, 2012, **12**, 2362–2366.
10 Q. Sun, Y. A. Wang, L. S. Li, D. Wang, T. Zhu, J. Xu, C. Yang and Y. Li, *Nat. Photonics*, 2007, **1**, 717–722.
11 X. Dai, Z. Zhang, Y. Jin, Y. Niu, H. Cao, X. Liang, L. Chen, J. Wang and X. Peng, *Nature*, 2014, **515**, 96–99.
12 Y. Lee, B. G. Jeong, H. Roh, J. Roh, J. Han, D. C. Lee, W. K. Bae, J.-Y. Kim and C. Lee, *Adv. Quantum Technol.*, 2018, **1**, 1700006.

13 Y. Sun, Y. Jiang, H. Peng, J. Wei, S. Zhang and S. Chen, *Nanoscale*, 2017, **9**, 8962–8969.
14 J. Pan, C. Wei, L. Wang, J. Zhuang, Q. Huang, W. Su, Z. Cui, A. Nathan, W. Lei and J. Chen, *Nanoscale*, 2018, **10**, 592–602.
15 W. K. Bae, Y.-S. Park, J. Lim, D. Lee, L. A. Padilha, H. McDaniel, I. Robel, C. Lee, J. M. Pietryga and V. I. Klimov, *Nat. Commun.*, 2013, **4**, 2661.
16 H. Lee, C.-M. Kang, M. Park, J. Kwak and C. Lee, *ACS Appl. Mater. Interfaces*, 2013, **5**, 1977–1981.
17 M. Kam, Q. Zhang, D. Zhang and Z. Fan, *Sci. Rep.*, 2019, **9**, 6963.
18 V. K. Sangwan, M. Zhu, S. Clark, K. A. Luck, T. J. Marks, M. G. Kanatzidis and M. C. Hersam, *ACS Appl. Mater. Interfaces*, 2019, **11**, 14166–14174.
19 X. Xu, Z. Xu, J. Tang, X. Zhang, L. Zhang, J. Wu and Z. Lan, *Chem. Eng. J.*, 2018, **351**, 391–398.
20 L.-C. Liu, J.-S. Chen, J.-S. Jeng and W.-Y. Chen, *ECS J. Solid State Sci. Technol.*, 2013, **2**, Q59–Q64.